CLIMATE-SPACE - THEME II: CROSS-ECV ACTIVITIES

ARCFRESH (ARCTIC FRESHWATER BUDGET)

Fit-for-purpose report (F4PR)

Prime & Science Lead: Ole Baltazar Andersen
DTU Space, Copenhagen, Denmark

Technical Officer: Anna Maria Trofaier, Sophie Hebden
ESA ECSAT, Didcot, United Kingdom

Consortium: DTU-Space, Department of Geodynamics (DTU)
ENVironmental Earth Observation IT GmbH (ENVEO)
Science and Technology AS (S&T)
Environment and Climate Change Canada Governmental (ECCC)
Norwegian Meteorological Institute (METNO)
Nansen Environmental and Remote Sensing Center (NERSC)
Norwegian Research Centre AS (NORCE)
National Physical Laboratory (NPL)
Swedish Meteorological and Hydrological Institute (SMHI)
University of Western Brittany (UBO)

Signatures page

Prepared by	Alex Cabaj Lead Author, ECCC	
Issued by	Daniele Fantin, Project Manager, S[&]T	
Checked by	Ole Baltazar Andersen Science Leader, DTU-S	
Approved by	Sophie Hebden ESA Technical Officer	

Table of Contents

Change Log

Issue	Author	Affected Section	Change	Status
0.5	D. Fantin, S&T	All	Document created	
1.0	A. Cabaj, ECCC	All	V 1.0 consolidated	Released to ESA

Acronyms and Abbreviations

CCI	Climate Change Initiative
CMEMS	Copernicus Marine Environment Monitoring Services
CPS	Climate Processes Section
CRD	Climate Research Division
DEM	Digital Elevation Model
DOT	Dynamic Ocean Topography
DTU	Technical University of Denmark
ECCC	Environment and Climate Change Canada
ECV	Essential Climate Variable
ENVEO	ENVironmental Earth Observation
EO	Earth Observation
ESA	European Space Agency
FWF	Freshwater flux
GCOS	Global Climate Observing System
GIS	Greenland Ice Sheet
GIS	Greenland Ice Sheet
GRACE	Gravity Recovery and Climate Experiment
IPCC	Intergovernmental Panel on Climate Change
IV	Ice Velocity
METNO	Norwegian Meteorological Institute
MFID	Mass Flux Ice Discharge
NERSC	Nansen Environmental and Remote Sensing Center
NORCE	Norwegian Research Centre
NPL	National Physical Laboratory
OBP	Ocean Bottom Pressure
PADB	Pan-Arctic Drainage Basin

RCM	RADARSAT Constellation Mission
S1	Sentinel-1
SAR	Synthetic Aperture RADAR
SEC	Surface Elevation Change
SIM	Sea Ice Motion
SMB	Surface Mass Balance
SMHI	Swedish Meteorological and Hydrological Institute
SoW	Statement-of-Work
SSH	Sea Surface Heights
SSS	Sea Surface Salinity
TBA	To be announced
TOPAZ	Towards an Operational Prediction system of the North Atlantic and the coastal Zone.
UBO	Université de Bretagne-Occidentale

1 Introduction

1.1 Applicable Document

This document contains the Fit-for-purpose report (F4PR) for the ARCFRESH project for CLIMATE-SPACE - THEME II: CROSS-ECV ACTIVITIES, in accordance with the contract [AD1], SoW [AD2] and proposal [AD3-AD10]. It is delivered as a part of WP2.

The purpose of this document is to provide a summary for the fit-for-purpose analysis and post-processing required for datasets to be used for the ARCFRESH product, along with uncertainty assessment.

1.2 Applicable Document Contents

This document is structured as follows:

- Chapter 1 introduces this document.
- Chapter 2 describes the objectives of the fit-for-purpose report
- Chapter 3 details the fitness-for-purpose and post-processing required for lateral fluxes (3.1, including river discharge, land ice, sea ice fluxes, and ocean gates), vertical fluxes (3.2, precipitation-evaporation), and validation data (3.3, including freshwater content and sea surface salinity)
- Chapter 4 describes the uncertainty assessment.

1.3 Applicable Documents

No	Doc. Id	Doc. Title	Date	Issue/ Revision/ Version
AD-1	4000145884/24/I-LR	ESA Contract No. 4000145884/24/I-LR	27/09/2024	NA
AD-2	ESA-EOP-SC-AMT-2023-21	Statement of Work and Annexes and Appendexes	01/12/2023	1.0
AD-3	DTU-ESA-ARCFRESH-CL-001	ARCFRESH Cover Letter	22/02/2024	1.0
AD-4	DTU-ESA-ARCFRESH-TPROP-001	ARCFRESH Technical Proposal	22/02/2024	1.0
AD-5	DTU-ESA-ARCFRESH-IPROP-001	ARCFRESH Implementation Proposal	22/02/2024	1.0
AD-6	DTU-ESA-ARCFRESH-MPROP-001	ARCFRESH Management Proposal	22/02/2024	1.0
AD-7	DTU-ESA-ARCFRESH-FPROP-001	ARCFRESH Financial Proposal	22/02/2024	1.0
AD-8	DTU-ESA-ARCFRESH-CPROP-001	ARCFRESH Contractual Proposal	22/02/2024	1.0
AD-9	DTU-ESA-ARCFRESH-BF-001	ARCFRESH Background and Facilities	22/02/2024	1.0
AD-10	DTU-ESA-ARCFRESH-CV-001	ARCFRESH Curricula Vitae	22/02/2024	1.0

Note: If not provided, the reference applies to the latest released Issue/Revision/Version

2 Objective of the Fit-for-purpose report

The objective of this task is to compile and collect all relevant datasets necessary for the method and algorithm development, validation, and scientific analyses within the project. We present in this report an assessment of the quality of the selected datasets, and conclude on their usefulness (i.e. their 'fit-for-purpose') for quantifying and investigating freshwater fluxes (FWF) in the Arctic Ocean. We also present a review of uncertainty information available for the datasets.

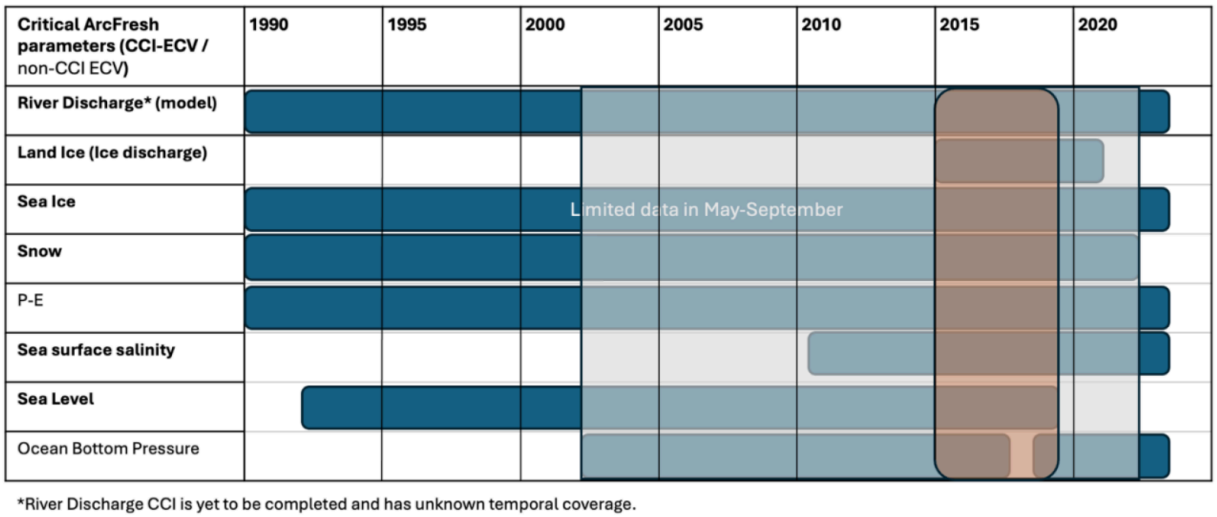

Figure 2.1. Temporal coverage of each critical ArcFresh parameter based on the inventory. The overlayed shaded areas indicate our 'golden' era (orange) and 'silver era' (grey). Note that for snow water equivalent, no products are available during the summer (June-September).

3 Fit-for-purpose analysis and required post-processing

The CCI ECV datasets offer a relatively brief common time series, spanning from 2015 to 2019, which we denote as our 'golden' period (indicated with orange colour in Figure 2.1), and we use this period as a criterion to assess if the relevant CCI ECVs are usable in their current state (i.e. fit-for-purpose). Post-processing refers to the conversion of ECVs into FWF with a uniform temporal resolution and a common uncertainty standard. This processing ensures that the datasets are directly comparable, facilitating a more straightforward analysis. General criteria for fitness-for-purpose include data coverage and availability (particularly during the 'golden' period), spatial and temporal resolution, data quality, and quantifiability of uncertainties. Specific descriptions of individual datasets may be further referenced from the ECV Inventory Document (EID).

Conceptually, there are two considerations for assessing the fitness for purpose for uncertainties: whether or not the uncertainty itself is fit for purpose (i.e. is the uncertainty of a given product sufficiently low to be useful), and whether or not the information about uncertainties is fit for purpose (i.e. is there sufficient information to adequately estimate uncertainties). At this stage it is difficult to assess what magnitude of uncertainty is 'low enough', and therefore within this study uncertainties are assessed in terms of the quality of information available about those uncertainties.

The ECV-database in task 2 (Deliverable 2.2) [R.3.2.2.2] will initially only contain ECVs with this 'golden' period (2015-2019) but will be updated when fluxes are extended as part of addressing ST1 in task 3 to task 5 (WP3-WP5), where we aim to determine all fluxes from 2003-2022 ('silver period'). The following sections contain a description of the fit-for-purpose and post-processing of ECVs to determine the fluxes mapped in Figure 2.1 for the 'golden' period.

3.1 Post-processing of lateral fluxes

3.1.1 River Discharge

River discharge freshwater fluxes are generated using a pan-Arctic hydrological model (Arctic Hydrological Predictions for the Environment, Arctic-HYPE) forced by the Hydrological Global Forcing Data (HydroGFD) precipitation and temperature analysis (Berg et al, 2021) and constrained by the available in-situ and satellite-based discharge (CCI River discharge; Arctic-HYCOS (Arctic Hydrological Cycle Observing System) and ArcticGRO (Arctic Great Rivers Observatory)) and snow (CCI Snow) data through data assimilation following Musuuza et al (2020). Arctic-HYCOS is a pan-Arctic collection of in-situ data compiled by the national hydrological services in the Arctic Council member states through the Arctic-HYCOS WMO project, whereas ArcticGRO is a component of the NSF (National Science Foundation) Arctic Observation Network. The datasets are complementary and all are needed to optimize the temporal and spatial coverage of the river discharge data and to hence satisfy the fit-for-purpose criteria. The Arctic-HYPE model represents the 23 million km^2 pan-Arctic drainage basin (PADB) by a network of about 30,000 sub-basins delineated using a 90 m resolution DEM (GWD-LR, Yamazaki et al, 2014). The average sub-basin size (700 km^2) corresponds roughly to a grid size of 25 × 25 km^2. The model output has a daily temporal resolution from 1979-present, and hence covers both the golden and silver periods. The outflow from a single model sub-basin represents the lateral water flux through a river cross-section at the defined by sub-basin outlet location in the river network. The outflow of inland sub-basins is used as inflow to their downstream sub-basin, whereas the outflow from the most downstream sub-basins corresponds to the river discharge into the ocean. The river discharge ECV representing the river freshwater inflow to the Arctic Ocean will thus be based on the discharge in the model sub-basins with outlet to the ocean only and will be further aggregated

to a suitable spatial resolution for the X-ECV analysis (1/10 of a degree, ~6km). For larger rivers, this means that the discharge might have to be distributed over several grid points in the spatially aggregated product, and in other cases, the discharge from several river outlets will be aggregated to a common grid point. The spatial, as well as the temporal aggregation to monthly timescale, will be made following the agreed protocols for uncertainty propagation (see Deliverable D4.1: Uncertainty Propagation Strategy (UPS)).

In addition to the flow-to-ocean product, data on river discharge and other internal variables such as CCI ECV daily snow water equivalent (from passive microwave and in situ data) and CCI ECV snow cover extent (from optical satellite data) will be provided for inland model sub-basins as needed for validation and uncertainty estimates, and other X-ECV investigations performed in later work packages. The snow water equivalent is at a 0.10° resolution, and the snow cover extent has a resolution of 0.01° during the golden and silver periods.

3.1.2 Land ice

The FWF contribution from land ice entails the sum of the solid ice discharge (D), e.g. ice draining and calving directly into the ocean, surface runoff (SR) and basal runoff (BR) from the land ice:

$$FWF_{land\_ice} = D + SR + BR$$

These components are assessed separately and combined to provide the overall FWF from land ice, with post-processing converting these components into fluxes that share a uniform temporal resolution and a common uncertainty standard.

To derive the surface runoff from the glaciated regions, we rely on output from two regional climate models: Modèle Atmosphérique Régional, (MAR) (Fettweis et al., 2017) and the Regional Atmospheric Climate Model (RACMO) (Noël et al., 2016). Specifically, we use the data as they are provided in Mankoff et al. (2020), which provides hourly runoff from defined ice sheet and land drainage basins as shown in Fig 3.1 (a). The data are available through 2024. Each model's output was regridded to the same 1 km grid using an offline statistical downscaling technique, and summed over the drainage basin outline. These model outputs are provided with uncertainties on runoff (15%) and drainage basin definition. Required post-processing includes aggregation of drainage basins (Fig 3.1(a)) to agree with those defined from ice flow patterns and basal flux (Karlsson et al., 2023). This allows for a consistent estimate of freshwater flux within the catchments relevant for ARCFRESH. We use the mean value of runoff from the two provided regional climate models, and integrate the temporal 1-day resolution provided by the models (as available in Mankoff et al., 2020) into time intervals relevant for ARCFRESH. In conclusion, we find that this dataset is well suited for ARCFRESH, although we note that similar datasets do not exist for the other ice caps that contribute freshwater to the Arctic Ocean, and we can take this into consideration in the error budget.

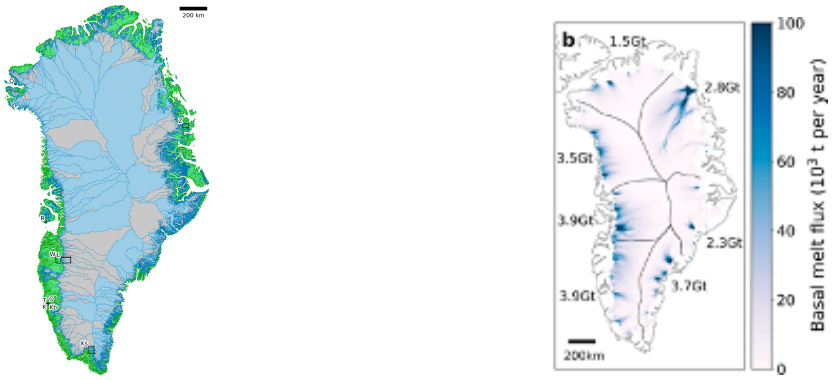

(a) (b)

Fig 3.1: (a) Drainage basin definitions from Mankoff et al., 2020. (b) Basal melt flux under the Greenland Ice Sheet. From Karlsson et al., 2021.

The basal melt and consequent runoff are generated by three processes: geothermal heat, frictional heat from ice flow and heat from surface melt input to the bed. A first constraint on basal melt fluxes under the Greenland Ice sheet was published by Karlsson et al., 2021, see Fig 3.3(b). Within the POLAR+ 4DGreenland project, this dataset was further developed, and in ArcFresh we employ this data set of monthly basal fluxes from the Greenland ice sheet's marine-terminating glaciers on a glacier–basin scale for the period 2010–2020 (Karlsson et al., 2023). The spatial and temporal resolution of this dataset makes it well suited for our analysis without any post-processing required. One issue is that the available dataset is only covering the Greenland Ice Sheet, and it excludes other glaciers and ice caps that generate an FWF into the Arctic Ocean. The dataset's temporal coverage of 2010–2020 covers the 'golden' period but does not cover the entire satellite era. The overall conclusion on the datasets to be used for quantifying the basal melt is that they are well suited – although not perfect – for the proposed analysis due to the issues raised.

The solid ice discharge FWF is calculated based on the time series of ice velocity in combination with an ice thickness model covering the flux gates (Morlighem et al., 2017). Year-round continuous ice velocity data covering the Greenland Ice Sheet margins (derived from repeat pass Copernicus Sentinel-1 SAR satellite data) has been available since October 2014 and has been used to calculate discharge for major outlet glaciers on a monthly time scale from Oct 2014 to Dec 2021 falling within the 'golden' period. Ice velocity coverage for other Arctic land ice masses is only available at lower temporal resolution due to limited Sentinel-1 acquisitions in these areas. Ice thickness observational data is scarce or non-existent in some regions but estimates of the cross-sectional areas of calving glaciers can also be made based on extrapolated data from radio-echo sounding (RES) or glacier freeboard/cliff heights derived from satellite or airborne altimetry (Blaszczyk et al., 2009; Wuite et al., 2015). To adjust the flux gate thickness over time, the surface elevation change data (SEC ECV from CCI Greenland Ice Sheet) can be employed (proposed in Option 2). This dataset can furthermore be used to correct for any mass changes that occur below a defined flux gate. These data are available over the entire Greenland Ice Sheet at 5km spatial resolution since 1992, making this dataset fully fit-for-purpose for aiding the solid ice discharge calculation on basin scale for the Greenland Ice Sheet within ArcFresh. The temporal resolution is 5 and 2-years (depending on altimetry missions), and the time period covered is 1992-present. A new dataset with monthly resolution for the years 2011-present based on CryoSat-2 data has recently been made available in CCI+ Greenland Ice Sheet – this dataset is currently under review in a submission to The Cryosphere – but the data is

available to ARCFRESH. One issue with the surface elevation change data is that it only covers the ice sheet and not e.g. Svalbard or the Russian Ice caps, which leaves an unmonitored part of the FWF. Dyurgerov et al. (2010) provides estimates of meltwater fluxes from both mountain glaciers/ice caps and the Greenland Ice Sheet indicating that this could amount to 40-45%.

In summary, the datasets currently available allow us to address all main components to calculate the FWF contribution from the Greenland Ice Sheet from Oct 2014 to Dec 2021. The fitness for purpose of the overall calculated ice sheet freshwater flux is directly determined by the fitness for purpose of these input datasets—discharge, basal melt, and surface runoff. Hence, we conclude that these datasets are fit-for-purpose for the ArcFresh project. Although Greenland is a major contributor in the Arctic, this leaves gaps and uncertainties in the contribution from other Arctic land ice masses. Narrowing down these knowledge gaps is the main objective of the work proposed in Option 2.

3.1.3 Sea ice fluxes

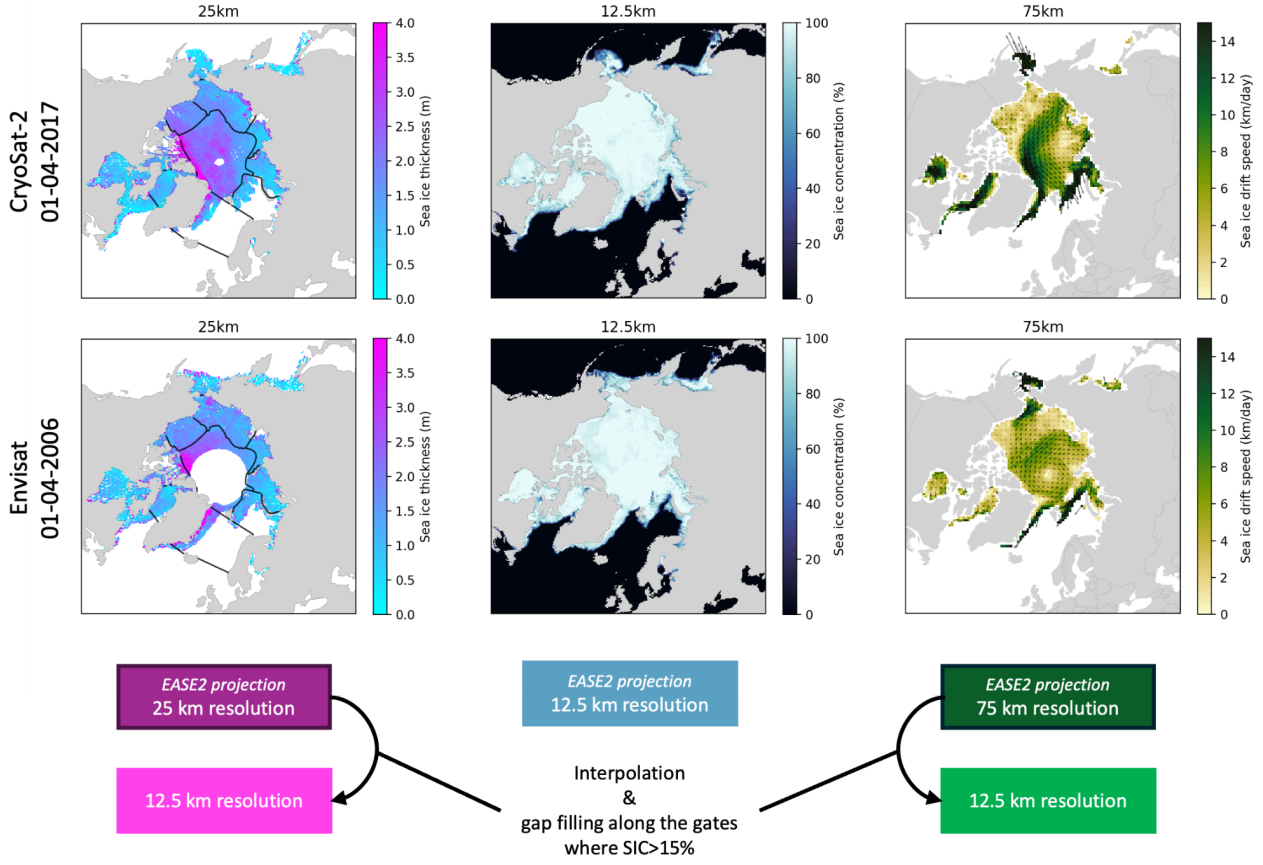

Figure 3.2: Maps of sea ice thickness, sea ice concentration, sea ice drift illustrating one month of the CryoSat-2 period (1st April 2017) and Envisat period (1st April 2006). The bottom panel shows the projection and the resolution

for each variable along with the processing preceding the sea ice volume fluxes computation. Black lines in the sea ice thickness represent the defined gates for fluxes calculation.

Sea ice volume flux $Q_{x,y}$ from gridded sea ice concentration, thickness and drift, in x and y directions of the projection coordinates is obtained by the following:

$$Q_{x,y} = GHCD_{x,y}$$

where G is the size of the grid cells, H is the sea ice thickness, C is the ice concentration and $D_{x,y}$ represents the ice drift in x and y directions respectively (Ricker et al., 2018). Averaging/resampling is performed for input products that have differing temporal or spatial resolutions as illustrated by Figure 3.2. Note that all the products are already on a daily basis, so temporal interpolation is not needed. Once the volume flux grids have been computed, the gates are discretized along their geometries. Flux is then interpolated from the grid onto these discrete segments, and the total flux through each gate is obtained by integrating over all segments. Once volume flux grids have been computed, fluxes through meridional and zonal gates are estimated by interpolation along those gates. The gate between the central Arctic region and the Laptev Sea is located within the polar coverage gap during the Envisat era. This affects a segment of approximately 300 km length. The satellite data coverage is limited in this area, so the gate may need to be slightly shifted or the flux field interpolated to fill the gap. Note that the required shift is roughly the width of a single grid cell, and thus remains within the uncertainty bounds. Thus, we do not expect this to have a substantial impact on the gate flux estimates. The sea ice volume fluxes will come as a daily value, one for each gate.

CCI ECV products provide sea ice thickness from satellite altimetry, drift-aware sea ice thickness, and sea ice concentration from microwave radiometry for the 'golden' period. Ice thickness is not available in May-September from the CCI products, and hence, they are not fully fit-for-purpose. However, year-round ice thickness can be supplemented by the altimetry-based Landy et al. (2022) year-round sea ice thickness product during the 'golden' period. The latter dataset is available on the Northern Polar Stereographic projection with a resolution of 80km on a bi-weekly basis, therefore, the dataset has to be regridded onto the 12.5km EASE2 grid and temporally interpolated to fit the 1-day basis. The OSI-SAF Global Low Resolution Sea Ice Drift provides daily sea ice drift from 1991-2020 at 75 km resolution. Aside from data gaps as mentioned above, all products satisfy the fit-for-purpose requirement of having at least a monthly temporal resolution. Each dataset of the altimetry sea ice thickness products, sea ice concentration, and low-resolution sea ice drift, is delivered with documented uncertainty estimates provided alongside the data, allowing for a complete uncertainty propagation. In terms of spatial coverage, CCI ECV altimetry products are provided at a 25 km resolution up to 81.4°N from 2002- 2010, and up to 88°N from 2011-present, and the SI-CCI high resolution CDR sea ice concentration is provided at a 12.5 km resolution. This resolution is sufficient to satisfy fit-for-purpose criteria.

Additional non-CCI sea ice motion data is provided from SAR, namely Sentinel-1A/B and the RADARSAT Constellation Mission (RCM), at a daily resolution for sea ice motion, and bi-weekly resolution for sea ice volume flux from 2016-present (Howell et al., 2022; Howell et al., 2024). These data provide more accurate ice drift, though with less spatial and temporal coverage during the "golden period" and are hence not fully fit-for-purpose. However, this data can serve as a reference and to help quantify uncertainties in the OSI-SAF sea ice drift.

3.1.4 Ocean gates

Determining freshwater fluxes across ocean gateways requires quantifying both the slope of the Dynamic Ocean Topography (DOT)—defined as the sea surface height (SSH) relative to the geoid—and the salinity content. The freshwater fluxes through the main Arctic and sub-Arctic gateways can be derived from the ESA CCI along-track product (Ablain et al., 2015) and the ESA CCI SLBC Arctic gridded sea level dataset (Rose et al., 2019), provided as weekly 0.25° × 0.5° grids. The along-track product spans 1993–2015, while the Arctic gridded product extends to 2018. Consequently, the CCI datasets only partially cover the "golden period" of consistent satellite altimetry.

For the ocean gateways located at or south of 66° N (Bering Strait, Davis Strait, Denmark Strait, and the Norwegian Sea Boundary), the slope of the DOT can be computed from along-track altimetry data from Jason-1 (2001–2009) and Jason-2 (2008–2017). These missions provide a 10-day repeat cycle, enabling flow estimates at a 10-day temporal resolution. An example of annual-averaged DOT and geostrophic slope across the Bering Strait is shown in Figure 3.3, while Figure 3.4 illustrates the corresponding fields across the Davis Strait compared with non-CCI RADS data of the same track/pass. The temporal evolution of the DOT slope and equivalent flow for the Canadian and Greenland sides of the Davis Strait is shown in Figure 3.5.

For the remaining external gateways (i.e. Fram Strait and the Barents Sea Opening), as well as for the internal Arctic gateways, the gridded DOT product is interpolated to the location of each gateway prior to slope calculation. An example based on the gridded CCI DOT product is given in Figure 3.6, which shows the monthly DOT slope across the Fram Strait, the mean DOT profile, and a map of the mean DOT with the gate outline.

Oceanic flow is estimated from the DOT data following the approach of Andersen et al. (2019) and hence are all SSH measurements referenced to the same geoid model (ESA OGMOC). The geostrophic approximation is valid only when inflow and outflow regions are treated separately, requiring sufficient across-strait spatial resolution. The high along-track resolution of Jason-1/2 is ideal for this purpose, while the gridded CCI product is mainly adequate for broader straits such as Fram Strait and the Barents Sea Opening.

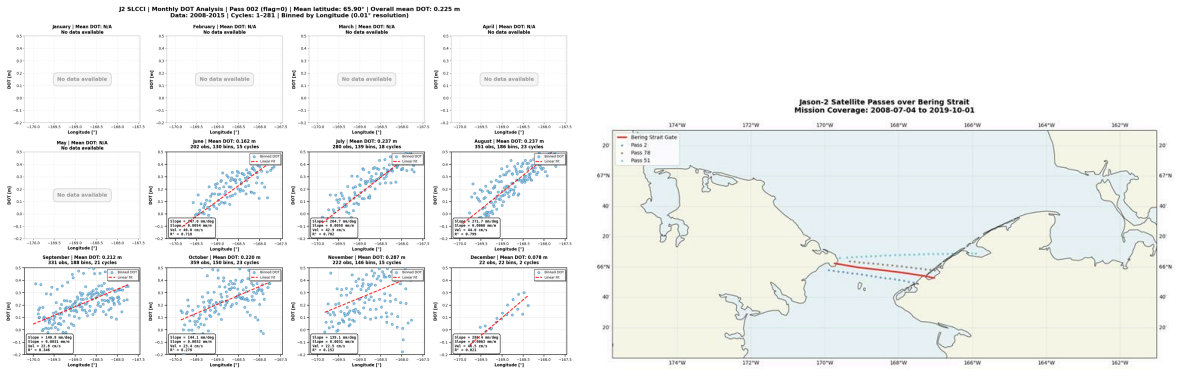

Figure 3.3. Annual averaged dynamic ocean topography from Jason-2 and the geostrophic slope across the Bering Strait.

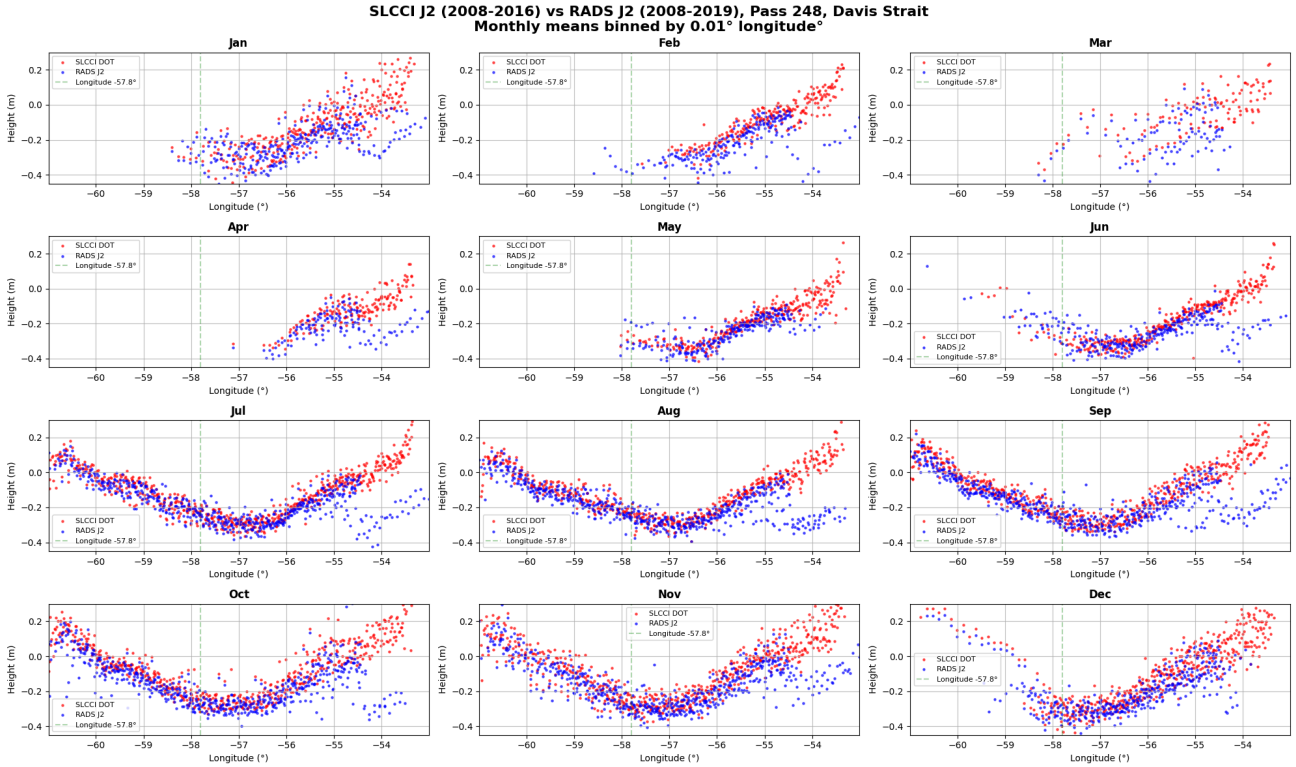

Figure 3.4. Annual averaged dynamic ocean topography from Jason-2 and the geostrophic slope across the Davies Strait and

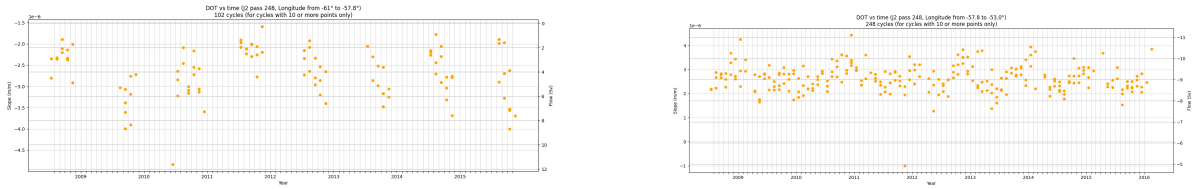

Figure 3.5 The timeseries of the DOT slope from Jason-2 and equivalent flow (assuming 200 m depth) for the Canadian side (left) and Greenland side (right).

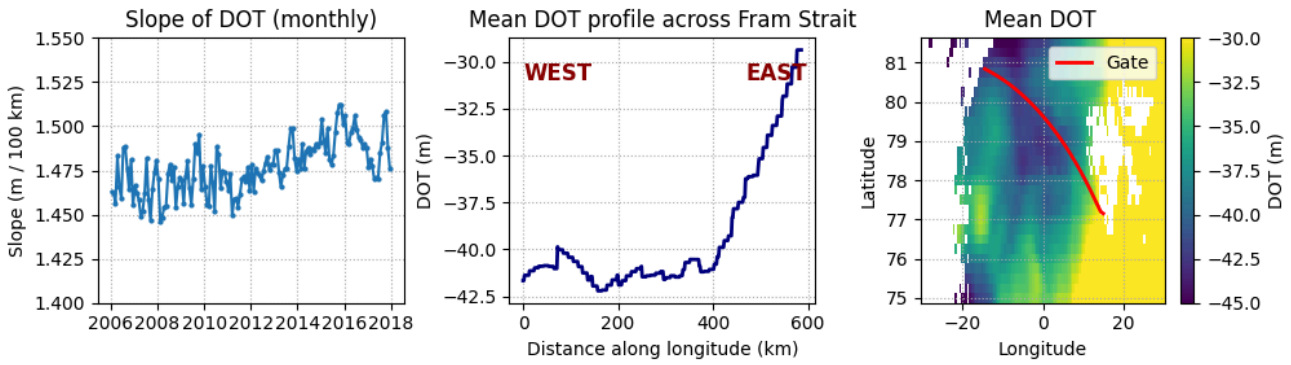

Figure 3.6 DOT across the Fram Strait based on the gridded SLCCI product. Left: time series of the monthly calculated DOT slope across the gate (longitudinal distance, not along-track). Middle: mean DOT profile. Right: Map of the mean DOT with the gate outline in red.

DOT slope gives the surface geostrophic flow, and—assuming negligible bottom pressure gradients—can be used to estimate depth-integrated baroclinic transport. Ocean Bottom Pressure (OBP) data from GRACE can provide complementary information on the barotropic component of the flow and, when combined with DOT, allow separation of the total (barotropic + baroclinic) transport (Peralta-Ferriz and Woodgate, 2023). However, the current ESA CCI GRACE dataset (ITSG2018) has a low spatial resolution and is not leakage-filtered, making it unreliable in coastal regions and thus unsuitable for use across ocean gateways. Hence, the geostrophic approximation from Andersen et al. (2019) is used, and we are currently not considering the method from Peralta-Ferriz and Woodgate (2023).

To estimate the freshwater content, depth-integrated salinity is required. However, as full-depth salinity observations are limited, the ESA CCI Sea Surface Salinity product is used to approximate the salinity field. For the Fram and Davis Straits, in situ observations from moorings and CTD profiles are incorporated to derive vertically integrated salinity and thus provide full-depth freshwater flux estimates. In the Fram Strait, the defined gate follows the track of Sentinel-3A and 3B altimeter data (not part of the CCI dataset). In the Davis Strait, the chosen gate coincides with the mooring section and is located approximately 50 km north of 66° N (limit of the Jason-1/2 tracks).

In summary, the current ESA CCI datasets enable an approximation of fluxes through all major ocean gateways. For the Davis and Bering Straits, the 10-day repeat altimetry allows geostrophic flow estimates with comparable temporal resolution from 2001 to 2015, partially covering the “silver period”, but insufficient for the “golden period”. For the larger Arctic gateways, the gridded CCI products provide sufficient spatial and temporal resolution to estimate transport, although not to resolve detailed boundaries of inflow and outflow in narrow straits. At present, CCI OBP data from GRACE cannot be used for transport estimation through narrow or coastal gateways due to their low spatial resolution and the absence of coastal leakage correction. The CCI along track data show a comparable quality to along-track RADS data (figure 3.4), hence suitable for the purpose. Additional along-track Sentinel-3A/B and possible CryoSat-2 data obtained from RADS are required to achieve optimal results across all gates.

3.2 Post-processing of vertical fluxes

3.2.1 Precipitation-Evaporation

Precipitation minus evaporation is a vertical flux that, in contrast to the lateral fluxes, is defined spatially for the pan-Arctic. We note that for the ArcFresh project, ESA CCI datasets are not used for P-E calculations, but we nevertheless provide some additional description of the data used and post-processing applied. The P-E FWF is derived from ERA5 reanalysis data. Although ERA5 P-E is associated with biases, it has been shown to outperform other reanalyses in the Arctic due to its high spatial resolution and data assimilation techniques (Barrett et al., 2020). Estimates of P-E in the Arctic based on ERA5 agree well with prior estimates (Ford and Frauenfeld, 2022). The Copernicus Arctic Regional ReAnalysis (CARRA) also provides hourly modelled P-E with a 2.5 km resolution. However, it does not cover the complete Arctic and does not provide uncertainty estimates.

The ERA5 precipitation and evaporation datasets are provided as gridded NetCDF files. Beyond basic spatial remapping and temporal averaging steps (from hourly to daily or monthly), post-processing will include masking of land and sea-ice areas for the Arctic and the sub-regions to derive the total P-E FWF over the open ocean. The deterministic ERA5 simulation (with 31 km resolution) will be used to estimate the P-E values from ERA5, while the 10-member ensemble (62 km resolution) is used to assess its uncertainty. The data from ERA5 are available at hourly temporal resolution during both the golden and silver periods.

3.3 Post-processing of validation data

3.3.1 Freshwater content

Changes in freshwater content (FWC) integrated over the Arctic Ocean correspond to the net freshwater flux entering and leaving through ocean gateways. Following the method of Giles et al. (2012), FWC anomalies are derived by combining GRACE-derived Ocean Bottom Pressure (OBP) with satellite altimetry-based Sea Surface Height (SSH) observations. The approach assumes a two-layer ocean, with a lighter surface layer overlying a denser deep layer of constant density. This method has been validated in the Beaufort Gyre (Giles et al., 2012) and along the Siberian Shelf (Armitage et al., 2016), but is less applicable in regions dominated by temperature-driven steric variability, such as the Barents Sea (Raj et al., 2020; Solomon et al., 2021).

The GRACE and GRACE-FO missions provide monthly OBP observations at a spatial resolution of approximately 300 km, which is suitable for monthly pan-Arctic estimates of FWC. The ESA CCI GRACE mascon (mass concentration) product developed by ITSG, is however not corrected for coastal leakage effects, meaning that a 300 km coastal filter needs to be applied to avoid signals of coastal mass changes (figure 3.7), and hence not suitable for the purpose of the STs in ArcFresh. We therefore rely on another GRACE mascon product (GSFC), which is coastal leakage corrected and provides full temporal resolution. An exception is the GRACE mission-gap (07/2017 - 08/2018), where we rely on interpolation while keeping the seasonality. For the finer temporal and spatial scales required in ST2 and ST3, GRACE data will be spatially and temporally interpolated to match the weekly, 0.25° × 0.5° gridded resolution of the ESA CCI Sea Level Budget Closure (SLBC) altimetry product (Rose et al., 2019, Figure 3.7), which is available until 2018. The altimetric coverage extends up to 82°N until 2010 and up to 88°N, and thereby near-full Arctic coverage from 2011-2018.

FWC changes are calculated within WP2 to ensure consistency with other Arctic freshwater flux estimates. The combined GRACE and altimetry datasets are sufficient for estimating pan-Arctic or basin-scale FWC variability at monthly to seasonal timescales, though the monthly GRACE-resolution does not allow for resolving any sub-monthly variations. Overall, the combined GRACE and CCI altimetry (2003–2018) provides adequate temporal and spatial coverage to produce reliable pan-Arctic freshwater content estimates for integration in WP2 for almost the entire golden period.

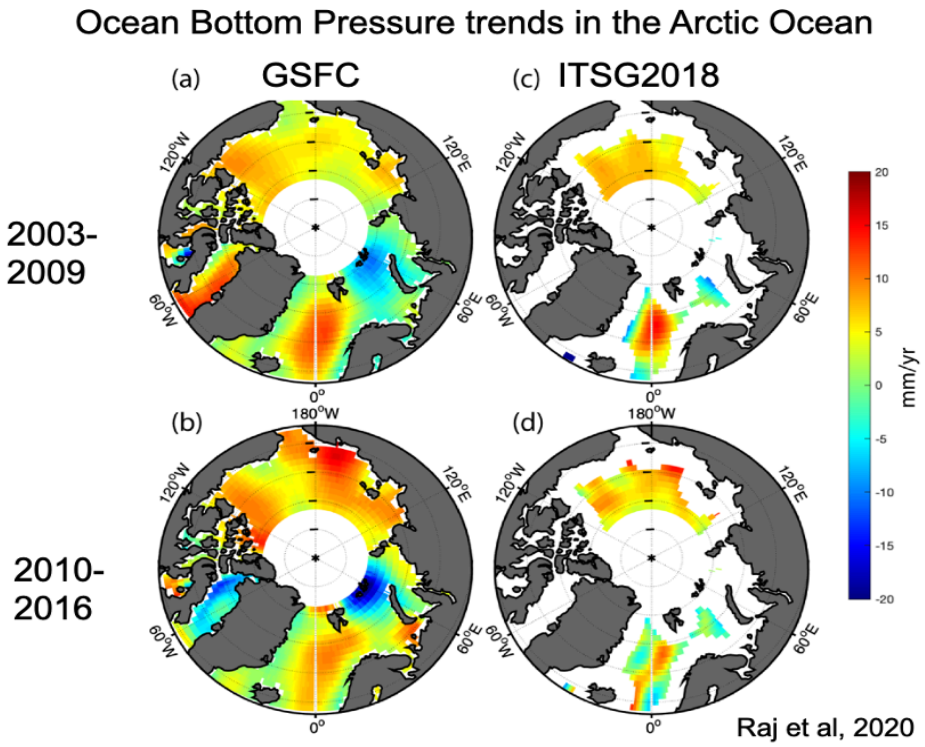

Figure 3.7: Ocean Bottom Pressure trends derived from GRACE for two time periods. Left column: Goddard Space Flight Center (GSFC) GRACE mascon product with leakage correction. Right column: ESA CCI (ITSG) product, where a coastal filter needs to be applied. Figure from Raj et al, 2020.

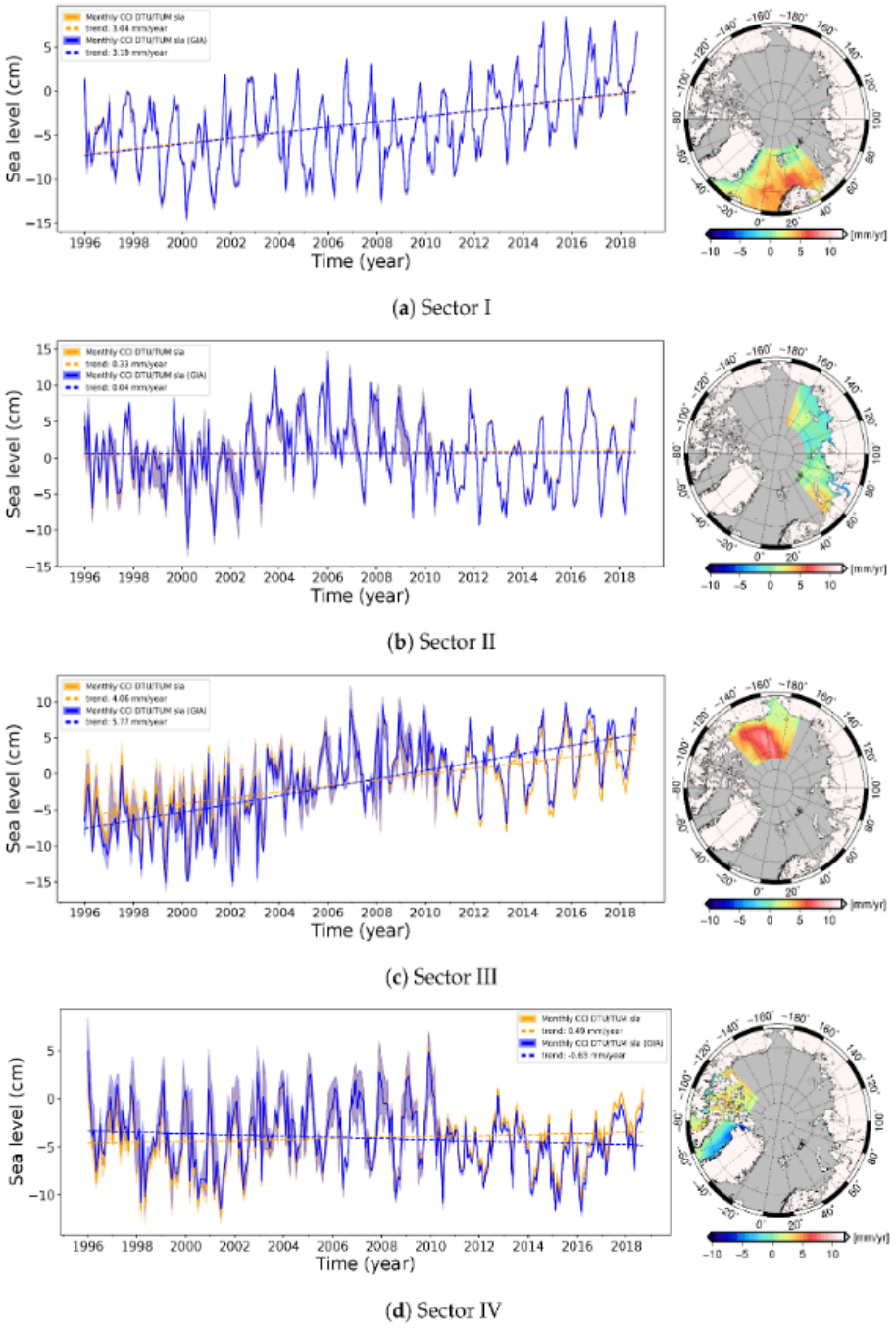

Figure 3.8. Arctic gridded sea level anomaly trends from ESA CCI (DTU/TUM) and time series for 4 Arctic regions (Rose et al, 2019). Figure from Rose et al, 2019.

3.3.2 Sea surface salinity

Sea surface salinity can be used as a proxy for freshwater content of the ocean column. In many regions of the Arctic Ocean (e.g. Siberian Shelves, Chukchi Seas) the SSS is well-related to the integral of freshwater content (Fournier et al., 2020). SSS can also be related to freshwater fluxes such as river discharge (Tarasenko et al., 2021) and sea ice melting flux (Supply et al., 2022, Van Straaten et al., 2025). This approach can be cross-validated using available in situ databases in the Arctic available such as UDASH (Behrendt et al., 2018), data collections from the International Council for the Exploration of the Sea (ICES), and all data available collected in the CORA dataset (https://doi.org/10.17882/46219).

We use SSS derived from L-band radiometric satellite observations. During the 'golden' period, datasets used to provide SSS include the CCI+SSS product and the SMOS Arctic CEC product. The latest version of the CCI+SSS product (v5.5) is provided at either weekly (7 days) or monthly resolution, and 45 km spatial resolution, provided along with a map of random uncertainty of around 0.5 pss (reduced to about 0.25 pss with the monthly products), provided along with the CCI+SSS fields. The CCI+SSSv5.5 product provides temporal coverage from 2010-2023. The SMOS Arctic CEC product is available from 2010-2023 at ~8-day and ~45 km resolution, and has an uncertainty of 0.5-1 pss. The CCI+SSS product merges two L-Band radiometer time series, i.e. the NASA SMAP and ESA SMOS missions, allowing for a better signal-to-noise ratio than one satellite alone, as in the SMOS Arctic CEC product. The CCI+SSS product is therefore more fit for purpose. Note that at high latitudes, land and ice contamination may also cause biases in the satellite SSS fields that can vary by time and region. An accurate estimation of the temporal and regional biases can be performed using comparisons against the available in situ measurements.

The freshwater content proxy using the CCI+SSS products is derived using the following approach:

- Satellite–In Situ SSS Comparison: comparing satellite sea surface salinity with in-situ salinity profiles.
- Upper-Layer Salinity vs. Freshwater Content: analyzing the relationship between near-surface/upper-layer salinity and freshwater content in the upper Arctic Ocean.
- Mode Extraction and Profile Reconstruction: extracting dominant modes from SSS and reconstructing vertical salinity profiles.

The first step was to gather the in situ profiles in a new comprehensive dataset over the Arctic Ocean for the purposes of validation and regression. In addition to UDASH and ICES, the new dataset includes the Siberian Shelves and Chukchi plateau where SSS is generally well correlated to SSS (Hall et al., 2023). The second step was to validate the CCI+SSS products using the enhanced in situ SSS dataset. Figure 3.9 shows the good correlation between the satellite SSS in the ice-free region during the summer season, i.e. the Beaufort Gyre, Siberian Shelf and Barents Sea. During the winter season, satellite SSS is only available in the Barents Sea, which is the only region free of ice during this season.

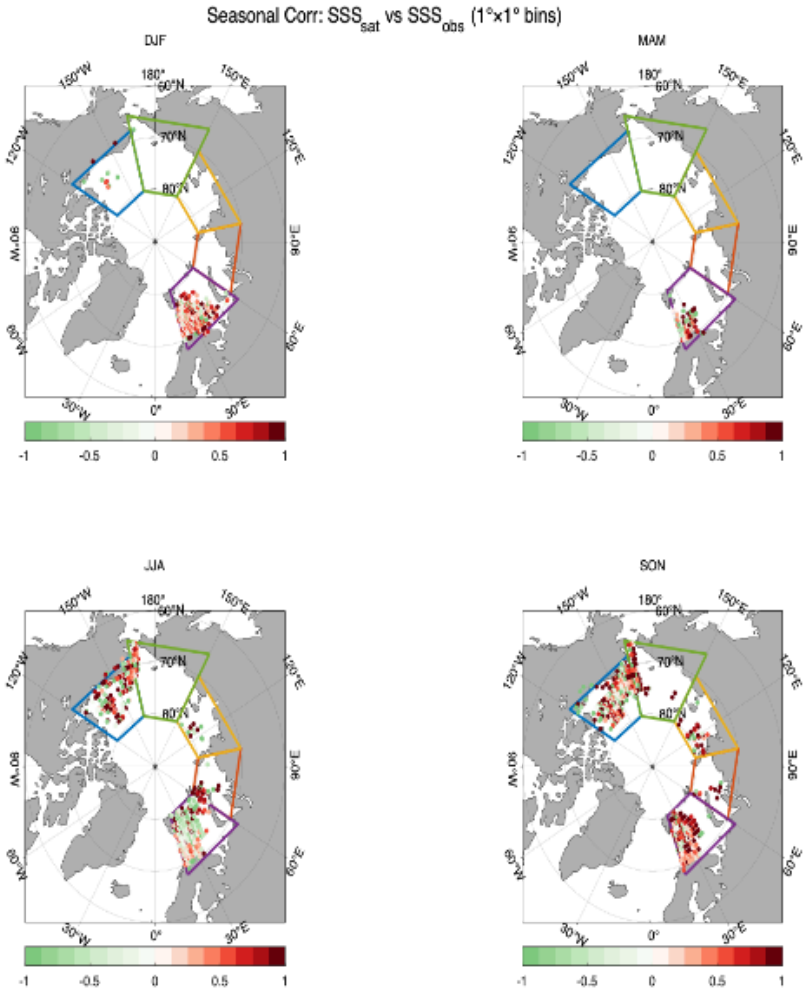

Figure 3.9 : Correlation between CCI SSS and local in situ measurements, data are binned seasonally over 1 degree (N>=2 per bin).

A study is ongoing to derive the relationship between the SSS and freshwater content over the water column. Figures 3.10 and 3.11 show the regional correlation between in situ SSS observations and the local freshwater content (over the upper 150 m depth). Significant anti-correlations are found in the Beaufort, Laptev and Kara Seas. However, anti-correlation appears to vary seasonally in the Barents Sea and over the Siberian Shelves (Figure 3.10). The anti-correlation is generally better on the shallow shelves and surrounding seas than in the deep Beaufort Basin (Figure 3.11). The next step will be to reconstruct salinity profiles and associated FW content using an EOF approach and applying this to CCI+SSS data to derive a FW proxy over the SSS satellite era and to fill the gap of missing direct FW estimates in the Arctic, especially on the Arctic shallow shelves.

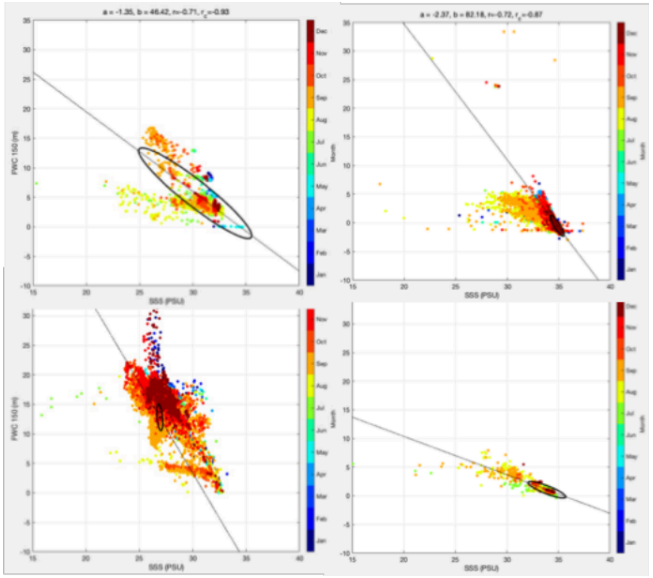

Figure 3.10: Scatter plot of SSS of in situ measurements against freshwater estimate in the top layer (150 m max) of the Arctic domain. Upper left : Siberian Shelf; upper right: Barents Sea; lower left: Beaufort Sea; lower right: Laptev and Kara Sea.

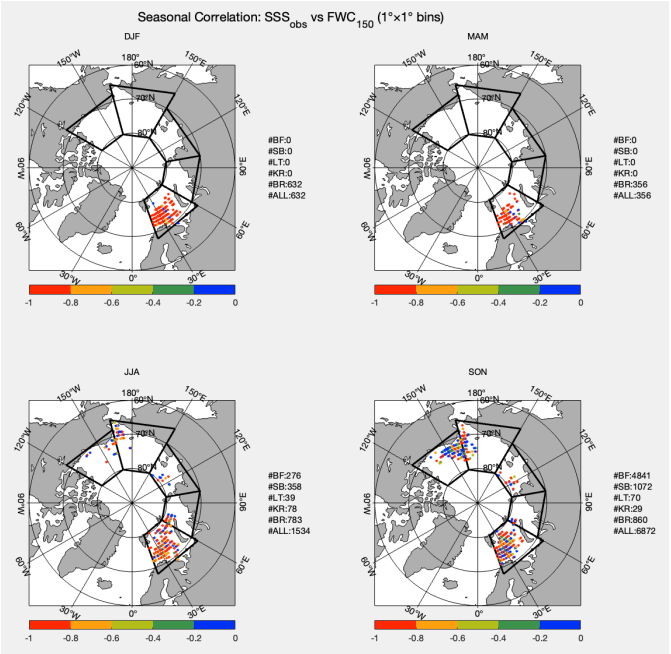

Figure 3.11 : Correlation between in situ SSS and local FWC, data are binned seasonally over 1 degree (N>=2 per bin)

4 Uncertainty assessment

The CCI-ECV datasets all come with an uncertainty assessment and uncertainty documentation. In assessing the 'fitness-for-purpose' of the uncertainty assessment, two related, but different, questions need to be asked. The first is whether the quoted uncertainties are small enough for the dataset to be fit for purpose to address the scientific topics. The second is whether the uncertainty evaluation and any information available on error-correlation structures is fit-for-purpose (sufficiently mature) for ingesting itself into an ocean model. The first step towards both these assessments is to review the uncertainty documentation of the relevant CCI-ECVs to understand what is available and to summarise that through an approach similar to the maturity matrices developed for satellite sensor data in EDAP [https://earth.esa.int/eogateway/activities/edap], or for FRMs (Goryl et al, 2023).

Answering the first question: whether the uncertainties associated with the data sets are sufficiently small for the data set to be useful for the scientific study, requires analysis from the perspective of the model. This work is discussed in the uncertainty propagation strategy document (D4.1 UPS).

Answering the second question requires an understanding of the maturity of both the uncertainty assessment and the error correlation information provided with the ECV data set. The maturity can be assessed in part by reviewing the ECV uncertainty report and understanding the basis of the analysis performed. It can also be assessed through statistical comparisons (including correlation studies) with independent observational data sets, for example in situ or airborne measurements. It is important to note that due to the complexity of Arctic observations, and the very limited availability of in situ and campaign data, we are not expecting a high maturity for uncertainty assessments for most ECV data sets. However, this review will identify which aspects can be considered more and which less reliable, and perhaps provide some information towards assessing the 'uncertainty of the uncertainty'. Note that quantitative assessments, and any work to make the uncertainty information more robust will be performed in WP4.

As well as this quantitative assessment of the 'fitness for purpose' of the uncertainty assessments, the project's review of data set uncertainties will document and report what terminology, and which variable names, are used for uncertainty information within the datasets. These will be aligned and, if necessary, translated to match the terminologies and variable names identified in WP1.

Beyond the uncertainties associated with the raw data, we need to consider the uncertainty associated with the transformations (spatial and temporal) required to convert data sets to a common grid for combining with the model. These uncertainties will include additional 'representation uncertainties' (see, e.g. Bulgin et al, 2022) as well as requiring the correct propagation of uncertainties and spatial and temporal error correlation structures through the regridding process. Within WP2, these issues will simply be reviewed and documented. Any efforts to quantify representation uncertainty and propagate uncertainties through regridding will be performed in WP4.

4.1 Review of uncertainty information in sea ice datasets

As described in Section 3.1.3, sea ice flux is a product of sea ice thickness, concentration and drift within each cell of a gridded product. As described in the ECV Inventory Document (EID), sea ice thickness (winter) and concentration are provided by ESA-CCI products, while drift uses two different observational non-CCI datasets (OSI-SAF drift from

microwave radiometry and the ECCC drift product from SAR). The uncertainty information available with each of these datasets are given below.

4.1.1 ESA CCI sea ice concentration

The ESA CCI+ sea ice concentration data product is used in this project for the evaluation of the sea ice concentration in the Arctic. This product uses passive microwave radiometer satellite data from various missions including: SSM/I, SSMIS, AMSR-E, AMSR2. Tie-points are "typical signatures of 100% ice and open water (0% ice) which are used in the sea ice algorithm". These are derived from training samples of known open water and assumed consolidated ice conditions.

The sea ice concentration product provides within the data file the observational values, the total uncertainty and two components of the uncertainty: the uncertainty associated with the algorithm (including instrument noise and tie-point variability) and the uncertainty associated with resampling. The two components can be added in quadrature to give the total uncertainty, and are therefore assumed to be independent. No explicit information is given on spatial or temporal error correlation. Information about these sources of uncertainty is given in the algorithm theoretical basis document (ATBD; Sea Ice CCI P1 ATBD-SIC D2.1 Issue 3.1).

In order to use the product within the ArcFresh project, we will need to estimate the spatial and temporal error correlation. That error correlation information is needed to support regridding first to the grid to be used for sea ice volume calculations, and then to integrate over the Arctic Ocean Gateways. Although this information is not available in the product, the ATBD provides information from which an initial estimate of the spatial/temporal error correlation can be made through expert judgement. For example, the tie points are described as being 'daily tie-points', which suggests a temporal error correlation of one day for that component. Similarly, the uncertainty associated with the radiative transfer model will contain a spatial/temporal error correlation component. Additionally, a recent paper (Wernecke, 2024) has considered spatial and temporal correlations in the SIC product. We therefore consider that there is sufficient information provided to include some such information in our analysis described in the Uncertainty Propagation Strategy (UPS) report.

4.1.2 ESA CCI sea ice thickness

The sea ice thickness is calculated from the satellite radar altimetry measurement of freeboard (the amount of ice above the water) and a calculation of thickness that considers sea ice density, snow density, snow depth and water density, where the ice density depends on the sea ice age, given from a 'sea ice type' file. The auxiliary datasets used are given in Table 2-1 of the Sea Ice CCI ATBD SIT D2.1.

Uncertainty values are given in the product files for all geophysical parameters (radar freeboard, (ice) freeboard, sea ice thickness and snow depth) for both product levels L2P and L3c). The uncertainties are propagated into the level 2 files based on different uncertainty components that are listed in the ATBD (Sea Ice CCI ATBD SIT D2.1). These are further propagated to level 3 (gridded products). The gridded products have an uncertainty that has taken spatial and temporal error correlation into account (at least at the systematic/random level). But error correlation of the gridded product itself (from grid-cell to grid-cell) is not given.

The uncertainty analysis for sea ice thickness is reasonably comprehensive and has some consideration of spatial and temporal error correlation information, and therefore is of value to the project.

4.1.3 Sea ice drift (OSI-SAF)

The OSI-SAF sea ice drift product is calculated from microwave radiometer (MR) measurements making use of image pairs and assessing the cross-correlation between the two through specific algorithms to maximise the identification of correlations. Additionally, the product makes use of a "free-drift model" to provide further clarity in the summer months (https://osi-saf.eumetsat.int/products/osi-405-c).

Uncertainties for this data product are provided as resolved X and Y components of the drift vectors. These uncertainties are evaluated as a combination of two major contributions from statistical validation and time mis-registration with the additional contribution of wind driven motion vectors for the summer melt season. The statistical validation is evaluated as a comparison between the resolved MR drift vectors and buoy motion measurements with magnitude of uncertainty being dependent on the provided "status_flag". The time mis-registration vectors are evaluated when two measurements of drift vectors are not time stamped. The wind motion vector uncertainties are evaluated similarly to statistical validation with a comparison to buoy drift data.

The uncertainty analysis for this product has been provided to some extent. To make use of this product within the ArcFresh product there will need to be more analysis provided for both temporal and spatial correlations required for regridding into the defined areas of interest within the Arctic. There has been some correlation analysis provided however as is inherent in the product.

4.1.4 Sea ice drift (ECCC)

The Environment and Climate Change Canada Automated Sea Ice Tracking System (ECCC-ASITS) is used to evaluate sea ice drift within the Arctic Ocean using Synthetic Aperture Radar (SAR) measurements for their increased accuracy over MR measurements. Similarly to MR measurements, sea ice drift is evaluated by taking image pairs and evaluating the correlation between the two. The methodology for this work can be found in the following paper (https://doi.org/10.5194/tc-16-1125-2022).

Uncertainties for this data product have been resolved as differences between evaluated sea ice drift vectors from SAR measurements and validation buoys. The evaluation of this uncertainty is further split into both summer and winter sea ice conditions. To provide uncertainties for the average evaluated sea ice drift vectors for a gridded cell area, individual uncertainties for the velocity vector are calculated and then these are summed for the entire desired area.

The uncertainty analysis has been considered for this product in the base extent of validation against drifting buoys, however explicit uncertainty analysis of spatial and temporal correlations will be required for use within the ArcFresh project.

4.1.5 Summer sea ice thickness from CS-2

Summer sea ice thickness is evaluated largely in the same way as with the sea ice thickness (see section 3.1.3). The methodology for this work is summarised in Landy et al. (2022).

The uncertainties for this data product are evaluated largely the same as for winter sea ice thickness. The small variations from the winter sea ice thickness result from the presence of melt ponds on top of the sea ice which both

affect the density levels of snow provided (and the associated uncertainty) and introduce a bias on the sea ice freeboard due to the lower overall height of the melt pond surface in relation to the sea ice.

The uncertainty analysis for sea ice thickness is reasonably comprehensive and has some consideration of spatial and temporal error correlation information, and therefore is of value to the project.

4.2 Land Ice

4.2.1 ESA CCI GIS: Annual Surface Elevation Change

The surface elevation change (SEC) measurements of Greenland ice sheets are performed by use of satellite radar altimetry. This is done by taking repeat measurements of the top surface of the snow/firn/ice. To ensure only anomalies of the SEC are being measured, a reference digital elevation model (DEM) is generally used.

Uncertainties for this data product have been provided with two key contributions from uncertainties in the SEC processor and from the deviations between the actual surface elevation change and the incorporated model into the processing. This is provided as a sum of both uncertainty contributions and are assumed to be independent.

To make use of the current uncertainty analysis provided with this data product within the ArcFresh project, the evaluation of both temporal and spatial correlations will need to be addressed. Partial temporal correlation analysis has been performed within the SEC product processing as can be seen within the ATBD (ESA GIS CCI ATBD V2.1) and further correlation analysis relating to the uncertainties can be performed with expert judgement.

4.2.2 ESA CCI GIS: Ice Velocity

Ice velocity measurements of the Greenland Ice Sheet are generally measured using Offset Tracking (OT). This makes use of features/aspects of both the ice and instrument signal in use of tracking the movement of the ice. This can be done by tracking features, waveform amplitude, coherence of waveform or the signal speckle. The ice velocity itself is evaluated using a similar method to sea ice velocity evaluation from the use of image pairs where the correlation between the two is calculated to inform the movement of the ice.

The uncertainties provided for this data product come from various different sources, including: general baseline errors, errors arising from coregistration, errors due to decorrelation, uncertainties in the ground control points, errors from phase unwrapping and errors from velocity inversion where the horizontal velocity of the ice must be imaged from multiple directions. The final provided uncertainty is given within the NetCDF file with the final data product; this uncertainty is an estimate of the standard deviation for a given pixel as seen in the end-to-end uncertainty budget (ESA CCI GIS E3UB v3.0). There is no explicit mention of spatial or temporal correlation analysis that is performed.

The uncertainty analysis for this product has been thought through fairly rigorously. Use within the ArcFresh project however will require the analysis of both spatial and temporal correlations between the evaluated products.

4.2.3 ESA CCI GIS: Mass Flux Ice Discharge

Mass Flux Ice Discharge (MFID) is the term given to the process of ice sheet loss due to solid ice discharge. Discharge for the Greenland Ice Sheet is evaluated at flux gates (collections of pixels which share a border over an outlet of the glacier) using the thickness of the ice taken from a DEM and a bedrock model and corrected for surface elevation change (SEC). The estimation of discharge is calculated from the product of ice velocity (assuming the depth averaged

velocity is equal to the surface velocity) and ice thickness (assuming negligible losses from basal uplift, erosion and melt) as the density of the ice is set to a known value.

The uncertainties for this product have been highlighted to come from five different data products: Ice thickness model, the variation in ice thickness, the depth averaged velocity of the ice, map projection uncertainties and finally software uncertainties. The uncertainties are provided with the MFID output product and provided in CSV format as the total uncertainty for this output as seen in the end-to-end uncertainty budget (ESA CCI GIS E3UB v3.0).

The use of this product within the ArcFresh project will require identification of temporal and spatial error correlations relating to the uncertainties. The uncertainties provided are thorough and cover all of the aspects as shown above.

4.2.4 NASA IceBridge: Greenland ice sheet thickness

The IceBridge Greenland BedMachine product provides information on Greenland bed topography and bathymetry. Within the product, ice sheet thickness is also derived and provided. The bed topography and overall ice thickness are generally evaluated using airborne radar sounders.

Uncertainties are provided within the netCDF datafile for this product however limited information is provided on how these uncertainties are calculated or where they come from. There is indication on the key sources of error such as from the “ice velocity direction and magnitude, surface mass balance errors and thinning rates”. It is identified that errors present from fjords may be significant. (IBMG UG v5.0)

Using this product within the ArcFresh project will involve possible investigation into the origins and quantification of uncertainty sources where possible. The knowledge of spatial and temporal correlations in the observations would also be applicable in understanding the contribution of this to the MFID to further understand its contribution to the gridded areas of the Arctic as defined within this project.

4.3 River Discharge

River discharge is the volume of water passing through a cross-section of a river over a given time. A common approach for monitoring river discharge is to measure the water level and transform it to discharge using a so-called stage-discharge relationship (also known as a rating curve). Stage discharge relationships can be obtained using direct measurements of the river discharge at different water levels and/or by hydraulic modelling. Direct measurements of river discharge can be done by measuring the water velocity at different points in the cross-section (to estimate the cross-section mean velocity) and multiplying with the cross-section area (which requires information about the cross-section bathymetry and the water level). Other techniques are available involving dilution of salts or other trace substances. The main point is that direct measurements of discharge are usually not applied for monitoring, but needed to establish monitoring based on water level measurements.

4.3.1 ESA CCI River Discharge

The ESA CCI River discharge data has been produced using satellite altimetry data and/or multispectral images. In both cases, the transformation from the satellite data to discharge is dependent on reference data to establish the necessary transformation relationships (eg. rating curves for the altimetry based method). The evaluation of uncertainties relating to this product have been covered within the ATDB document (CCI Discharge ATBD v1.1) with in-depth description of

contributions to the combined uncertainty and evaluated whilst using the law of propagation of uncertainties (LPU). Uncertainties relating to this product are provided alongside the data in the full output dataset in a CSV format.

The uncertainties within this data product have been considered and evaluated rigorously. Inclusion of spatial and temporal correlation effects would be worth investigating for the ArcFresh project.

4.3.2 In-situ River Discharge data

The in-situ river discharge data from Arctic-HYCOS and ArcticGRO datasets do not provide any quantitative uncertainty information, which is typical for these types of data. Thus, assumptions on the uncertainties in these data have to be made when assimilating it in the modelling. Relative uncertainty of about 15%-30% are commonly used, but depending on the quality of the rating curves for specific stations and flow conditions, even higher values are also possible. A conservative estimate would be in the range 15-30%.

4.3.3 ESA CCI Snow: Snow water equivalent

Snow water equivalent (SWE) is the mass of snow per unit area which is converted to its equivalent in water. This is most generally measured from microwave radiometer combined with in situ measurements of snow depth at weather stations.

The SWE data product is provided in a NetCDF file with the estimate of SWE and a statistical standard deviation of SWE estimates as seen in the ATBD (Snow CCI ATBD v4.0). A full evaluation of the uncertainty relating to the snow water equivalent CCI product can be found within the Snow CCI E3UB (end-to-end uncertainty budget) document v4.0. This captures all of the contributions to the combined total uncertainty in detail.

This data product will be valuable to use within the ArcFresh project as the uncertainties have been evaluated in detail with documentation. However, further investigation or evaluation of spatial or temporal correlations will also be required for all observations to improve overall uncertainty estimations within the Arctic gridded areas.

4.4 Precipitation-Evaporation

Neither precipitation, evaporation nor precipitation-evaporation is a CCI-ECV, and there are no CCI datasets for these parameters. However, some non-CCI EO and reanalysis precipitation and evaporation datasets are available and will be discussed in the following sub-sections. Note however that, since these are not CCI datasets, no detailed fit-for-purpose analysis or extended uncertainty quantification is performed for these datasets. In the Arctic region, the EO datasets are affected by large biases or uncertainties, and EO evaporation and precipitation are often not consistent with each other as they are from different satellite missions. Conversely, reanalysis data from e.g. ERA5 provides consistent precipitation and evaporation.

4.4.1 Infrared, microwave and rain gauges from GPCP v1.3

This data product is used to evaluate daily surface precipitation from 1996 onwards on a 1 degree global grid. This can be completed using microwave radiometers (specifically SSM/I and SSMIS), the atmospheric infrared sounder (AIRS) and in situ gauges. The description for the data product can be found within the daily ATBD (GPCP ATBD Daily) however a more full description can be found in the monthly ATBD (GPCP ATBD Monthly).

Description of error estimation is only included within the monthly ATBD document and is only given for the case of merging satellite data with the in situ rain gauges in the form of random effects. Suggested targets for the overall random and systematic errors are provided within the product user guide page (GPCP Product User Guide v1.3).

To use this product within the ArcFresh project it would be useful to investigate the origins of the contributions to the provided uncertainty whilst also trying to identify other sources of uncertainty. The spatial and temporal correlations particularly between the satellite microwave radiometer measurements would be useful to estimate.

4.4.2 Infrared and microwave from GIRAFE

The Global Interpolated Rainfall Estimation (GIRAFE) provides the precipitation data on a 1 degree global grid from passive microwave observations from polar orbiting satellites with the addition of geostationary satellites providing infrared observations around the equator. The main description for the algorithm used in evaluation can be found in the product's ATBD document (SAF GIRAFE ATBD v1.3).

The uncertainty for this data product is given as the uncertainty on the final accumulated precipitation as a function of the daily sampling error of the precipitation. The contributions to this uncertainty are mentioned to come from calibration, the algorithm and the sampling (area and timings). There is no description on the evaluation of these contributions to the final uncertainty. The sampling error is provided within a netCDF file along with the daily accumulated precipitation (SAF GIRAFE PUM v1.1) where the total final uncertainty on the precipitation is evaluated using this sampling error (SAF GIRAFE ATBD v1.3).

Investigation into the origins of the contributions to the total final uncertainty would be useful to carry out when using this product within the ArcFresh project. Understanding of the spatial and temporal correlations between the passive microwave measurements would also be useful to investigate as none have been provided with the data product currently.

4.4.3 Microwave from COBRA

The Copernicus Microwave-Based Global Precipitation (COBRA) product provides gridded, level 3, monthly estimates of precipitation rates on a 1 degree global grid for the period 2000-2017. Data for these measurements are provided by multiple instruments including: SSM/I, SSMIS, AMSR-E and the TMI instruments. The full algorithm is provided within the product's algorithm theoretical basis document (COBRA ATBD v1.1).

Uncertainties relating to this product are only provided as part of the output data in the form of a daily standard deviation based on the mean precipitation rates calculated as the collaboration of all microwave instrument products. Documentation pertaining to the collation of all the data is not provided, however there are target requirements in the product user guide for the systematic and random contributions to the uncertainty (COBRA PUG v1.1).

Investigation into the origins of the contributions to the total final uncertainty would be useful to carry out when using this product within the ArcFresh project. Understanding of the spatial and temporal correlations between the passive microwave measurements would also be useful to investigate as none have been provided with the data product currently.

4.4.4 Various EO sensor evaluation from OAFlux V3.0

The Objectively Analysed Air-Sea Fluxes (OAFlux) project provided latent heat flux and evaporation estimates over daily gridded 1 degree cells over the period of 1 January 1985 to 31 December 2009 and has been validated against in situ flux measurements. The full algorithm description can be found in the technical report for the OAFlux project (WHOI OAFlux TD v3.0).

Uncertainties within the technical documentation are provided as the errors on the daily latent and sensible heat fluxes (of which evaporation can be calculated). There is no discussion as to what input data feeds into the errors and no consideration of correlation effects.

Investigation into the origins of the contributions to the total final uncertainty would be useful to carry out when using this product within the ArcFresh project. Understanding of the spatial and temporal correlations from the observations used in the algorithm would also be useful, particularly in the evaluation of the daily heat fluxes.

4.4.5 Microwave radiometry from HOAPS v4.0

The Hamburg Ocean-Atmosphere Parameters and Fluxes from Satellite Data (HOAPS) data product provided estimations for latent heat flux, evaporation, precipitation, freshwater flux and near surface specific humidity, wind speed and total column water vapour at 6-hourly, 0.5° resolution covering 80°S to 80°N from Jul 1987 to Dec 2014. The algorithm for the data product is described within the algorithm theoretical basis document (CM SAF HOAPS ATBD v4.0).

Uncertainties relating to the evaporation product have been rigorously discussed within the algorithm theoretical basis document which evaluates sources of error with their respective uncertainties and uses covariance analysis to provide correlations between uncertainties. The final uncertainties are provided with the NetCDF file and are split into systematic and random error information with the inclusion of standard deviation.

The HOAPS dataset could be a very valuable product within the ArcFresh project as it provides P-E together with fit-for-purpose uncertainties. However, the dataset does not cover the required time period nor the complete Arctic region.

4.4.6 Reanalysis data from ERA5

Data from the ECMWF atmospheric reanalysis ERA5 (Hersbach et al., 2020) are provided with hourly temporal resolution from 1940 onwards on a 0.25° global grid, including precipitation and evaporation. The data is generated by the use of a numerical model with advanced data assimilation techniques. Uncertainty for these data products is given as the uncertainty resulting from a 10-member simulation ensemble, propagating the uncertainties in the observational data assimilated through the modelling system.

The uncertainty analysis for ERA5 is described in detail at https://confluence.ecmwf.int/display/CKB/ERA5%3A+uncertainty+estimation. The description is reasonably comprehensive but the uncertainty does not account for all sources such as systematic modelling errors or correlated errors. Thus the uncertainty provided along the ERA5 data is likely to underestimate the real uncertainty.

To calculate P-E (precipitation minus evaporation), P and E should be consistent with each other to close the FWF budget in terms of vertical fluxes. From the datasets listed above, only ERA5 provides both variables consistently (within

the numerical modelling framework) for the whole golden (2015–2019) and silver (2003–2022) period, and covering the complete Arctic.

4.5 Ocean Gateways

4.5.1 Sea level from radar altimetry (Jason 1-3 & S6MF)

Sea level anomalies (SLA) are measured predominantly by use of satellite radar altimeters. These are the key anomalies in the level relative to the general mean sea surface height as evaluated in reference to the Earth's ellipsoid. For this product, processing of the SLAs is found in the RADS data manual V4.0.

This product has no dedicated uncertainty analysis documentation however the data manual does identify the key corrections that are applicable to satellite radar altimeter measurements such as: the dry and wet tropospheric corrections, the ionospheric correction and the atmospheric correction. The data manual also highlights how these corrections are implemented and references as to where corrections come from. The nominal uncertainty provided within the EID document is ~3 cm range uncertainty.

For the ArcFresh project it would be important to investigate this further to get a final applied uncertainty to each measurement that can be applied to each gridded area. Investigation into spatial and temporal correlations between the measurements would also be useful.

4.5.2 Sea level from radar altimetry (Sentinel-3)

The Sentinel-3 radar altimetry product also provides sea level anomaly measurements. For this product, processing of the SLAs is found in the Sentinel-3 L1 DG v1.3 & Sentinel-3 L2 DG V1.3.

Uncertainty given within the EID document is provided as ~ 3 cm on the range. A list of desired goal and requirement maximum values for each error contribution and maximum correction are provided within the data guide Sentinel-3 L1 DG v1.3 & Sentinel-3 L2 DG V1.3. Further information surrounding these can be found here S3 SRAL altimetry processing baseline V5.

Nominal uncertainties given in the EID with limited information about the evaluation of said uncertainty. Further investigation of the origins of uncertainties, along with spatial and temporal correlation effects, would be useful to contribute to the ArcFresh project.

4.5.3 Salinity from CTD and Moorings

Measurements of sea water salinity can be carried out by underwater moorings and conductivity temperature depth sensors (CTDs) in the Arctic Ocean. The moorings are mostly specific sections of the Arctic ocean whereas the CTDs can be deployed in multiple regions.

The data product for the CTD only provides the salinity measurements and corrections required for these measurements but does not include the uncertainties or methodologies to evaluate the uncertainties (CTD Data Documentation). Little information is provided in the datasheet for the moorings.

Investigation into both the origins and quantification of uncertainties relating to the CTD would be required for this product. Correlation effects relating to the CTD will also be required.

4.6 Sea level and ocean bottom pressure

4.6.1 ESA CCI Sea Level: High latitude sea level anomalies from satellite altimetry

Sea level anomalies are measured predominantly by use of satellite radar altimeters. These are the key anomalies in the level relative to the general mean sea surface height as evaluated in reference to the Earth's ellipsoid.

The uncertainties relating to this data product are described within the error characterisation report (ESA CCI SL Error Report V2.2) and are mostly attributed to the corrections required for the radar for the different mediums that interact with it as it travels through, corrections such as: the ionospheric correction, wet and dry tropospheric corrections etc. There is however no final uncertainty provided within the data product file.

The corrections for this data product have been rigorously discussed and applied to the final data product. No uncertainty evaluation can be found within the general or the specific dataset (SL CCI CCN5 DTU TUM ArcticDataset2) . For the ArcFresh project it would be important to investigate this further to get a final applied uncertainty to each measurement that can be applied to each gridded area. Investigation into spatial and temporal correlations between the measurements would also be useful.

4.6.2 ESA CCI Sea level: FCDR 2.0

The ESA CCI Fundamental Climate Data Records of sea level anomalies and altimeter standards, Version 2.0 (FCDR 2.0) product also provides sea level anomaly measurements. The uncertainties relating to this data product are described within the error characterisation report (ESA CCI SL Error Report V2.2) and are mostly attributed to the corrections required for the radar for the different mediums that interact with it as it travels through, corrections such as: the ionospheric correction, wet and dry tropospheric corrections etc. There is however no final uncertainty provided within the data product file.

The corrections for this data product have been rigorously discussed and applied to the final data product. No uncertainty evaluation can be found within the general or the specific dataset (ESA CCI SL PUG FCDR v2.2) but temporal and spatial contributions to the uncertainty in the mean sea level can be found within the NetCDF for the output product. For the ArcFresh project investigation into spatial and temporal correlations between the measurements would also be useful.

4.6.3 ESA CCI Sea Level: High latitude sea level anomalies for Envisat and SARAL/AltiKa

The Envisat and SARAL/AltiKa missions also provide SLA measurements. The uncertainties relating to this altimetry data product are described within the error characterisation report (ESA CCI SL Error Report V2.2) and are mostly attributed to the corrections required for the radar for the different mediums that interact with it as it travels through, corrections such as: the ionospheric correction, wet and dry tropospheric corrections etc. There is however no final uncertainty provided within the data product file.

The corrections for this data product have been rigorously discussed and applied to the final data product. No uncertainty evaluation can be found within the general or the specific dataset (ESA CCI SL Envisat SARAL v1.0). For the ArcFresh project it would be important to investigate this further to get a final applied uncertainty to each measurement that can be applied to each gridded area. Investigation into spatial and temporal correlations between the measurements would also be useful.

4.6.4 ESA CCI Sea Level Budget: High latitude sea level anomalies from satellite altimetry

Uncertainties relating to the ESA CCI Sea Level Budget altimetry product are described within the error characterisation report (ESA CCI SL Error Report V2.2) and are mostly attributed to the corrections required for the radar for the different mediums that interact with it as it travels through, corrections such as: the ionospheric correction, wet and dry tropospheric corrections etc. There is however no final uncertainty provided within the data product file.

The corrections for this data product have been rigorously discussed and applied to the final data product. No uncertainty evaluation can be found within the general or the specific dataset (ESA CCI SL Envisat SARAL v1.0). For the ArcFresh project it would be important to investigate this further to get a final applied uncertainty to each measurement that can be applied to each gridded area. Investigation into spatial and temporal correlations between the measurements would also be useful.

4.6.5 ESA CCI sea level budget: Ocean bottom pressure from GRACE and GRACE-FO

The ocean bottom pressure measurements taken by TU Graz (Graz university of technology) have minimal algorithms available with this product, documentation only found to be formal description and algorithm document (Description and Algorithm document).

No uncertainty evaluation is mentioned within the documentation or found in relation to this product, and therefore this product would not be fully fit-for-purpose for this project.

4.6.6 Sea surface height measurements from CryoTempo enhanced polar Ocean CryoSat-2

The sea surface heights as part of the CryoTempo project evaluated from CryoSat-2 are created as part of the project as ancillary data used in the evaluation of sea ice freeboard for example. The full algorithm documentation can be found in the Cryo-Tempo technical product handbook (CryoTEMPO TPH v4.1).

Uncertainties are mentioned within the product handbook but no description of the evaluation or calculation is provided. Correlations are not mentioned to have been considered. The uncertainty for the sea level anomalies are provided with the main product within the NetCDF file.

For the ArcFresh project it would be useful to investigate the origin of the uncertainties associated with this data product as well as to investigate spatial and temporal correlation effects between measurements.

4.6.7 Ocean bottom pressure from NASA Goddard Space Flight Center

The ocean bottom pressure product from NASA is provided within the Estimating the Circulation and Climate of the Ocean (ECCO) product. This product estimates the ocean bottom pressure from the ocean pressure via use of the GRACE and GRACE-FO missions. Some of the estimation can be found within the product user guide (ECCO UG V4.4).

Specific errors relating to the ocean bottom pressure are not explicitly mentioned within the documentation.

Further investigation will be required to evaluate the origin of uncertainties relating to ocean bottom pressure measurements. No explicit mention of correlations between observations is given so this would be useful to investigate.

4.7 Sea surface salinity

4.7.1 ESA CCI sea surface salinity: sea surface salinity from SMOS, SMAP, Aquarius L-band microwave

Sea surface salinity (SSS) is measured by L-band microwave radiometers on the SMOS, SMAP and Aquarius satellites. The full algorithm for each level product for evaluation of SSS is found in the ESA CCI ATBD (ESA CCI SSS ATDB v5.1).

The uncertainties associated with each level product are rigorously discussed within the CCI End-to-End ECV Uncertainty Budget document (ESA CCI SSS E3UB v5.0). Both systematic and random contributions to the uncertainty have been broken down in detail into their individual contributing components. However, no correlations between uncertainties have been discussed relating to these measurements. The final uncertainty has been given as 0.5 pss (practical salinity scale).

The uncertainty information given for individual uncertainties is rigorously evaluated and will be of use to this project. It would be useful to investigate correlation effects between observations.

4.7.2 Sea surface salinity from SMOS band microwave

Sea surface salinity (SSS) is measured by L-band microwave radiometers on the SMOS, SMAP and Aquarius satellites. The full algorithm for the dielectric constant used to derive the level-3 SMOS SSS over the Arctic Ocean is found in the ESA CCI ATBD (SMOS L2OS ATBD) with the derivation to get to SSS found in Boutin et al. (2023).

The uncertainties have also been provided briefly within Boutin et al. (2023). The uncertainty has been estimated between 0.5-1.0 pss (practical salinity scale). Further investigation into temporal and spatial correlations between observations would be useful to do.

5 References

Ablain, M., Cazenave, A., Larnicol, G., Balmaseda, M., Cipollini, P., Faugère, Y., Fernandes, M. J., Henry, O., Johannessen, J. A., Knudsen, P., Andersen, O., Legeais, J., Meyssignac, B., Picot, N., Roca, M., Rudenko, S., Scharffenberg, M. G., Stammer, D., Timms, G., and Benveniste, J.: Improved sea level record over the satellite altimetry era (1993–2010) from the Climate Change Initiative project, Ocean Sci., 11, 67-82, doi:10.5194/os-11-67-2015, 2015.

Andersen, O. B., Mertikas, S. P., Pail, R., & others. (2019). Arctic freshwater fluxes from Earth observation data. In S. Mertikas & R. Pail (Eds.), Fiducial Reference Measurements for Altimetry (Vol. 150). Springer, Cham. https://doi.org/10.1007/1345_2019_75

Armitage, T. W. K., Bacon, S., Ridout, A. L., Thomas, S. F., Aksenov, Y., & Wingham, D. J. (2016). Arctic sea surface height variability and change from satellite radar altimetry and GRACE, 2003-2014.

Barrett, A. P., Stroeve, J. C., & Serreze, M. C. (2020). Arctic Ocean precipitation from atmospheric reanalyses and comparisons with North Pole drifting station records. Journal of Geophysical Research: Oceans, 125(1), e2019JC015415. https://doi.org/10.1029/2019JC015415

Behrendt, A., Sumata, H., Rabe, B., & Schauer, U. (2018). UDASH–unified database for Arctic and Subarctic hydrography. Earth System Science Data, 10(2), 1119-1138. https://doi.org/10.5194/essd-10-1119-2018

Berg, P., Almén, F., & Bozhinova, D. (2021). HydroGFD3.0 (Hydrological Global Forcing Data): a 25 km global precipitation and temperature data set updated in near-real time. Earth System Science Data, 13(4), 1531–1545. https://doi.org/10.5194/essd-13-1531-2021

Blaszczyk, M., Jania, J., & Hagen, J. O. (2009). Tidewater glaciers of Svalbard: Recent changes and estimates of calving fluxes. Polish Polar Research, 30(2), 85–142.

Boutin, J., Vergely, J., Bonjean, F., Perrot, X., Zhou, Y., Dinnat, E. P., Lang, R. H., Vine, D. M. L., & Sabia, R. (2023). New seawater dielectric constant parametrization and application to SMOS retrieved salinity. IEEE Transactions on Geoscience and Remote Sensing, 61, 1–13. https://doi.org/10.1109/tgrs.2023.3257923

Bulgin, C. E., Thomas, C. M., Waller, J. A., & Woolliams, E. R. (2022). Representation uncertainty in the Earth sciences. Earth and Space Science, 9, e2021EA002129. https://doi.org/10.1029/2021EA002129

Dyurgerov, M., Bring, A., & Destouni, G. (2010). Integrated assessment of changes in freshwater inflow to the Arctic Ocean. Journal of Geophysical Research, 115, D12116. https://doi.org/10.1029/2009JD013060

Fettweis, X., Box, J.E., Agosta, C., Amory, C., Kittel, C., Lang, C., Van As, D., Machguth, H. and Gallée, H., 2017. Reconstructions of the 1900–2015 Greenland ice sheet surface mass balance using the regional climate MAR model. The Cryosphere, 11(2), pp.1015-1033.

Ford, V. L., & Frauenfeld, O. W. (2022). Arctic precipitation recycling and hydrologic budget changes in response to sea ice loss. Global and Planetary Change, 209, 103752. https://doi.org/10.1016/j.gloplacha.2022.103752

Fournier, S., Lee, T., Wang, X., Armitage, T. W. K., Wang, O., Fukumori, I., & Kwok, R. (2020). Sea surface salinity as a proxy for Arctic Ocean freshwater changes. Journal of Geophysical Research: Oceans, 125, e2020JC016110. https://doi.org/10.1029/2020JC016110

Giles, K. A., Laxon, S. W., Ridout, A. L., Wingham, D. J., & Bacon, S. (2012). Western Arctic Ocean freshwater storage increased by wind-driven spin-up of the Beaufort Gyre. Nature Geoscience, 5(3), 194–197. https://doi.org/10.1038/ngeo1379

Goryl, P., Fox, N., Donlon, C., & Castracane, P. (2023). Fiducial reference measurements (FRMs): What are they? Remote Sensing, 15(20), 5017. https://doi.org/10.3390/rs15205017

Howell, S. E. L., Babb, D. G., Landy, J. C., Moore, G. W. K., Ballinger, T. J., McNeil, K., et al. (2024). Baffin Bay ice export and production from Sentinel-1, the RADARSAT Constellation Mission, and CryoSat-2: 2016–2022. Geophysical Research Letters, 51, e2024GL111364. https://doi.org/10.1029/2024GL111364

Howell, S. E. L., Brady, M., & Komarov, A. S. (2022). Generating large-scale sea ice motion from Sentinel-1 and the RADARSAT Constellation Mission using the Environment and Climate Change Canada automated sea ice tracking system. The Cryosphere, 16(3), 1125–1139. https://doi.org/10.5194/tc-16-1125-2022

Karlsson, N.B., Mankoff, K.D., Solgaard, A.M., Larsen, S.H., How, P.R., Fausto, R.S. and Sørensen, L.S., 2023. A data set of monthly freshwater fluxes from the Greenland ice sheet's marine-terminating glaciers on a glacier–basin scale 2010–2020. GEUS Bulletin, 53, p.8338.

Karlsson, N. B., Solgaard, A. M., Mankoff, K. D., Gillet-Chaulet, F., MacGregor, J. A., Box, J. E., Citterio, M., Colgan, W. T., Larsen, S. H., Kjeldsen, K. K., Korsgaard, N. J., Benn, D. I., Hewitt, I. J., & Fausto, R. S. (2021). A first constraint on basal melt-water production of the Greenland ice sheet. Nature Communications, 12(1). https://doi.org/10.1038/s41467-021-23739-z

Landy, J. C., Dawson, G. J., Tsamados, M., Bushuk, M., Stroeve, J. C., Howell, S. E. L., Krumpen, T., Babb, D. G., Komarov, A. S., Heorton, H. D. B. S., Belter, H. J., & Aksenov, Y. (2022). A year-round satellite sea-ice thickness record from CryoSat-2. Nature, 609(7927), 517–522. https://doi.org/10.1038/s41586-022-05058-5

Mankoff, K.D., Noël, B., Fettweis, X., Ahlstrøm, A.P., Colgan, W., Kondo, K., Langley, K., Sugiyama, S., Van As, D. and Fausto, R.S., 2020. Greenland liquid water discharge from 1958 through 2019. Earth System Science Data, 12(4), pp.2811-2841.

Morlighem, M., Williams, C. N., Rignot, E., An, L., Arndt, J. E., Bamber, J. L., … Zinglersen, K. B. (2017). BedMachine v3: Complete bed topography and ocean bathymetry mapping of Greenland from multibeam echo sounding combined with mass conservation, *Geophysical Research Letters*, 44, 11,051–11,061. https://doi.org/10.1002/2017GL074954

Musuuza, J. L., Gustafsson, D., Pimentel, R., Crochemore, L., & Pechlivanidis, I. (2020). Impact of satellite and in situ data assimilation on hydrological predictions. Remote Sensing, 12(5), 811. https://doi.org/10.3390/rs12050811

Noël, B., Van De Berg, W.J., Machguth, H., Lhermitte, S., Howat, I., Fettweis, X. and Van Den Broeke, M.R., 2016. A daily, 1 km resolution data set of downscaled Greenland ice sheet surface mass balance (1958–2015). The Cryosphere, 10(5), pp.2361-2377.

Peralta-Ferriz, C., & Woodgate, R. A. (2023). Arctic and sub-Arctic mechanisms explaining observed increasing northward flow through the Bering Strait and why models may be getting it wrong. Geophysical Research Letters, 50, e2023GL104697. https://doi.org/10.1029/2023GL104697

Raj, R., Andersen, O., Johannessen, J., Gutknecht, B., Chatterjee, S., Rose, S., Bonaduce, A., Horwath, M., Ranndal, H., Richter, K., Palanisamy, H., Ludwigsen, C., Bertino, L., Nilsen, J. Ø., Knudsen, P., Hogg, A., Cazenave, A., & Benveniste, J. (2020). Arctic Sea Level Budget Assessment during the GRACE/Argo Time Period. Remote Sensing, 12(17), 2837. https://doi.org/10.3390/rs12172837

Ricker, R., Girard-Ardhuin, F., Krumpen, T., & Lique, C. (2018). Satellite-derived sea ice export and its impact on Arctic ice mass balance. The Cryosphere, 12(9), 3017-3032.

Rose, S. K., Andersen, O. B., Passaro, M., Ludwigsen, C. A., & Schwatke, C. (2019). Arctic Ocean Sea Level Record from the Complete Radar Altimetry Era: 1991–2018. Remote Sensing, 11, 1672. https://doi.org/10.3390/rs11141672

Solomon, A., Heuzé, C., Rabe, B., Bacon, S., Bertino, L., Heimbach, P., Inoue, J., Iovino, D., Mottram, R., Zhang, X., Aksenov, Y., McAdam, R., Nguyen, A., Raj, R. P., & Tang, H. (2021). Freshwater in the Arctic Ocean 2010–2019. Ocean Science, 17, 1081–1102. https://doi.org/10.5194/os-17-1081-2021

Supply, A., Boutin, J., Vergely, J.-L., Kolodziejczyk, N., Reverdin, G., Reul, N., & Tarasenko, A. (2020). New insights into SMOS sea surface salinity retrievals in the Arctic Ocean. Remote Sensing of Environment, 249 , 112027.

Tarasenko, A., Supply, A., Kusse-Tiuz, N., Ivanov, V., Makhotin, M., Tournadre, J., Chaperon, Kolodziejczyk, N., & Reverdin, G. (2021). Properties of surface water masses in the Laptev and the East Siberian seas in summer 2018 from in situ and satellite data. Ocean Science, 17(1), 221–247.

Van Straaten, C., Lique, C., & Kolodziejcyk, N. (2025). The life cycle of the low salinity lenses at the surface of the Arctic Ocean. Journal of Geophysical Research Oceans, 130(4). https://doi.org/10.1029/2024jc021699

Wernecke, A., Notz, D., Kern, S., & Lavergne, T. (2024). Estimating the uncertainty of sea-ice area and sea-ice extent from satellite retrievals. ˜the œCryosphere, 18(5), 2473–2486. https://doi.org/10.5194/tc-18-2473-2024

Wuite, J., Rott, H., Hetzenecker, M., Floricioiu, D., De Rydt, J., Gudmundsson, G. H., Nagler, T., & Kern, M. (2015). Evolution of surface velocities and ice discharge of Larsen B outlet glaciers from 1995 to 2013. The Cryosphere, 9, 957–969.

Yamazaki, D., O'Loughlin, F., Trigg, M. A., Miller, Z. F., Pavelsky, T. M., & Bates, P. D. (2014). Development of the Global Width Database for large rivers. Water Resources Research, 50(4), 3467–3480. https://doi.org/10.1002/2013wr014664